Stimulated Raman scattering with a Gaussian pump beam in H_2 gas

S. Lögl, M. Scherm, and Max Maier
Naturwissenschaftliche Fakultät II–Physik, Universität Regensburg, D-93040 Regensburg, Germany
(Received 7 November 1994)

Raman scattering of the $Q(1)$ line in H_2 gas was investigated from the spontaneous to the stimulated scattering region using a frequency-doubled Q-switched Nd:YAG laser (where YAG denotes yttrium aluminum garnet). We measured the Raman Stokes energy as a function of the laser power and the radial distribution of the Stokes intensity for the unfocused and the focused Gaussian laser beam. There is good agreement between the experiments and the results of a nonorthogonal mode theory in the region of stimulated Raman scattering. For cell lengths short compared to the Rayleigh range of the laser beam or for Raman cells far from the beam waist, stimulated Raman scattering is described in a good approximation by an adapted plane-wave theory. In the region of spontaneous Raman scattering, the measured dependence on cell length, solid angle, and focusing conditions is not in accordance with the nonorthogonal mode theory, but agrees with the standard theory of spontaneous Raman scattering.

PACS number(s): 42.65.Dr, 42.55.Ye, 42.50.Lc, 33.20.Fb

I. INTRODUCTION

Since the first observation of stimulated Raman scattering (SRS) numerous investigations on experimental and theoretical aspects of this effect have been published (for a review see [1–5]). For quasistationary SRS the comparison between measurements and calculations has been hampered by various problems. In many Raman active substances there are competing nonlinear processes, e.g., self-focusing of laser light [6] and stimulated Brillouin scattering [7]. In media such as H_2 gas and liquid N_2, where SRS is the dominant process, an unexpected steep rise of the Raman Stokes energy as a function of laser intensity has been measured [8–11]. An explanation of this effect was given in terms of feedback by diffuse reflections from the cell windows and optical elements [12–14]. It was shown that for Raman cells longer than the laser pulse length, SRS showed no anomalous behavior [14]. Therefore, from the experimental point of view H_2 gas in a long cell is a suitable medium for the comparison of theory and experiments of SRS.

Most of the theories developed for SRS are based on plane waves [1–5]. However, in the experiments, the pump laser beam has a radial and axial intensity distribution; for example, often the lowest-order mode with a Gaussian radial distribution is used. The problem is to adapt the plane-wave theories to the real experimental situation. Various approaches to the problem of focused laser beams have been treated in the literature [15–19]. Recently, a nonorthogonal mode theory of Raman scattering with a focused laser beam was presented [20], which described quantitatively SRS in H_2 gas under various experimental conditions [14,20].

In this paper we present the results of theoretical and experimental investigations of stationary Raman scattering in H_2 gas from the spontaneous to the stimulated scattering region (excluding saturation). The experiments on SRS were carried out with a frequency-doubled Q-switched Nd:YAG laser (where YAG denotes yttrium aluminum garnet) with a long H_2 cell (824 cm) to avoid feedback problems. We measured the Raman Stokes energy as a function of the laser power and the radial intensity distribution of the Stokes beam for different experimental conditions. The experimental results are compared with the results of the nonorthogonal mode theory [20]. In addition, we discuss the conditions under which the measurements are described correctly by an appropriate adapted plane-wave theory. Particular emphasis is given to spontaneous Raman scattering where the easurements are compared with both the nonorthogonal mode theory [20] and the standard theory of spontaneous Raman scattering [21].

In Sec. II the main results of the nonorthogonal mode theory of SRS for the Raman gain, the Stokes power, and the radial intensity distribution of the Stokes beam are described. Sections III and IV treat adapted plane-wave theories and the comparison with the nonorthogonal mode theory, respectively. In Sec. V the results of the calculations of spontaneous Raman scattering using the nonorthogonal mode theory and the standard theory are compared. The experimental setup is described in Sec. VI. The experimental results on spontaneous and stimulated Raman scattering are compared with the theoretical calculations in Sec. VII. The conclusions are given in Sec. VIII.

II. NONORTHOGONAL MODE THEORY

The nonorthogonal mode theory of Raman scattering with focused laser beams has been treated in detail in Refs. [15,20]. In the following a brief description of the underlying principles and the main results, which are needed for the discussion of the experiments, is given.

A. Solution of the wave equation

The electric-field operator for a Stokes wave traveling in the z direction can be written as

$$\hat{E}_S(t,z,\vec{r})=\hat{E}_S^{(+)}(z,\vec{r})\exp[i(k_S z-\omega_S t)] + \hat{E}_S^{(-)}(z,\vec{r})\exp[-i(k_S z-\omega_S t)] , \quad (1)$$

where k_S and ω_S are the wave vector and the frequency of the Raman Stokes light. The amplification of the Stokes field, whose amplitude is assumed to vary slowly with distance z, is described by the wave equation in the steady-state paraxial limit.

$$\left[\nabla_T^2-2ik_S\frac{\partial}{\partial z}+ik_S g(z,r)\right]\hat{E}_S^{(-)}(z,\vec{r})=-4\pi k_S^2\hat{P}_{\rm sp}^{\dagger}(z,\vec{r}) , \quad (2)$$

where $\nabla_T^2=\partial^2/\partial x^2+\partial^2/\partial y^2$ and $g(z,r)$ is the Raman gain. To account for spontaneous scattering, a quantum Langevin operator $\hat{P}_{\rm sp}^{\dagger}(z,\vec{r})$ has been included, which represents the quantum fluctuations in the polarization of the medium. We treat a laser beam with power P_L and a radial and axial intensity distribution $L_L(z,r)$, which is described by the lowest-order Gauss-Laguerre mode of the free space (see below). In this case, the spatial nonuniform gain is given by

$$g(z,r)=g_0 I_L(z,r)=g_0\frac{P_L}{r_0^2(z)\pi}\exp[-r^2/r_0^2(z)] . \quad (3)$$

g_0 is the Raman gain factor and $r_0(z)$ is the $1/e$ radius of the radial intensity distribution of the laser beam, which is connected to the spot size $w_0(z)$ of the laser field by $r_0(z)=w_0(z)/\sqrt{2}$. The z dependence of the laser beam radius is given by

$$r_0^2(z)=r_0^2(0)[1+(z/z_0)^2] . \quad (4)$$

$r_0(0)$ is the radius in the beam waist and z_0 is the Rayleigh range, equal to one-half of the confocal parameter. For the lowest-order Gauss-Laguerre mode U_0^0 they are related by

$$z_0=k_L r_0^2(0) , \quad (5)$$

where k_L is the wave vector of the laser light.

The presence of the gain term in Eq. (2) makes the wave equation non-Hermitian. To solve the wave equation, the amplified Stokes field is expanded into a set of nonorthogonal modes

$$\hat{E}_S^{(-)}(z,\vec{r})=\sum_{n,l}\hat{a}_n^{l\dagger}(z)\phi_n^l(z,\vec{r}) , \quad (6)$$

where $\hat{a}_n^{l\dagger}$ is a generalized creation operator for photons in the nonorthogonal mode $\phi_n^l(z,\vec{r})$. The modes are required to satisfy the eigenvalue equation

$$\left[\nabla_T^2-2ik_S\frac{\partial}{\partial z}+ik_S g(z,r)\right]\phi_n^l(z,\vec{r}) = \lambda_n^l\frac{2ik_S}{k_L r_0^2(z)}\phi_n^l(z,\vec{r}) . \quad (7)$$

λ_n^l is the eigenvalue associated with the mode $\phi_n^l(z,\vec{r})$. The indices n and l correspond to the radial and the angular degrees of freedom, respectively.

It has been shown [15,20] to be useful to expand the modes $\phi_n^l(z,\vec{r})$ in terms of the free-space Gauss-Laguerre modes $U_n^l(z,\vec{r})$ which satisfy the free-space paraxial wave equation and are complete and orthogonal modes. Substituting the expansion

$$\phi_n^l(z,\vec{r})=\sum_p b_{n,p}^l U_p^l(z,\vec{r}) \quad (8)$$

into Eq. (7) and using the orthogonality relation for the U_n^l leads to a differential equation for the free-space coefficients $b_{n,p}^l$, which are, in general, complex. To simplify this equation the variable z is changed to the propagation variable

$$\theta=\tan^{-1}(z/z_0) . \quad (9)$$

In addition, the free-space coefficients are written as

$$b_{n,p'}^l=\exp(-i2p'\theta)\chi_{n,p'}^l . \quad (10)$$

Using Eqs. (7)–(10) we arrive at a system of coupled eigenvalue equations for $\chi_{n,p'}^l$

$$(2ip'-\lambda_n^l)\chi_{n,p'}^l+\tfrac{1}{2}\mu G_{Rr}\sum_p\chi_{n,p}^l Q_{p',p}^l(\mu)=0 , \quad (11)$$

where the mode filling factor μ, the Raman gain G_{Rr} within the Rayleigh range, and the polynomial $Q_{p',p}^l$ will be defined below. With the solution of this system the Raman Stokes modes can be written as

$$\phi_n^l(z,\vec{r})=\sum_p\exp[-i2p\tan^{-1}(z/z_0)]\chi_{n,p}^l U_p^l(z,\vec{r}) . \quad (12)$$

In Eq. (11) the Raman gain G_{Rr} within the Rayleigh range z_0 is given by

$$G_{Rr}=g_0 I_L(0,0)z_0 , \quad (13)$$

where $I_L(0,0)$ is the laser intensity in the center of the beam waist (at $z=0$ and $r=0$). Introducing the laser power P_L, the laser intensity can be written as $I_L(0,0)=P_L/[\pi r_0^2(0)]$. Using this expression and Eq. (5) we get for the Raman gain G_{Rr} within the Rayleigh range

$$G_{Rr}=k_L g_0 P_L/\pi . \quad (14)$$

G_{Rr} is independent of the Rayleigh range z_0, i.e., it is independent of the focusing conditions, but it depends on the laser power P_L. The mode filling factor μ is defined as

$$\mu=k_S/(k_S+k_L) . \quad (15)$$

$Q_{p',p}^l(\mu)$ is a polynomial in μ, which has been calculated in Ref. [15] for the case that $g(z,r)=g_0 P_L|U_0^0(z,r)|^2$. This corresponds to the Gaussian intensity distribution of the laser beam given in Eq. (3).

As a consequence of the non-Hermitian nature of the wave equation the usual power orthogonality conditions do not hold for the modes $\phi_n^l(z,\vec{r})$. They are supplanted by

$$\int d^2r\, \phi_m^{l*}\phi_n^j=\delta_{l,j}\sum_p \chi_{m,p}^{l*}\chi_{n,p}^j=\sum_p \chi_{m,p}^{l*}\chi_{n,p}^l=B_{n,m}^l \ . \quad (16)$$

Equation (16) represents a measure of the overlap between the nonorthogonal modes. The quantity $(B_{n,n}^l)^2$ is referred to as the excess noise factor [22] or Petermann factor [23] and is equal to or greater than unity.

There is a biorthogonality relationship with another set of modes $\psi_n^l(z,\vec{r})$, referred to as adjoint modes. They are obtained from the solution of the Hermitian adjoint of the differential operator in Eq. (7). The biorthogonality condition is given by

$$\int d^2r\, \psi_m^{l*}\phi_n^l=\delta_{m,n} \ . \quad (17)$$

Using the properties of the biorthogonal modes, Eq. (17) can be written as

$$\sum_p \chi_{m,p}^l\chi_{n,p}^l=\delta_{m,n} \ . \quad (18)$$

This equation is used to normalize the eigenfunctions $\chi_{n,p}^l$, which are solutions of the eigenvalue equation (11).

After the modes ϕ_n^l of the Raman generator have been determined, the z dependence of the operators $\hat{a}_n^{l\dagger}$ has to be found. Substituting the field expansion Eq. (6) into the wave equation (2) leads to an equation of motion for $\hat{a}_n^{l\dagger}$,

$$\sum_n \phi_n^l\left[\frac{\partial \hat{a}_n^{l\dagger}}{\partial z}-\frac{\lambda_n^l}{k_L r_0^2(z)}\hat{a}_n^{l\dagger}\right]=-2\pi i k_S \hat{P}_{\rm sp}^{\dagger}(z,\vec{r}) \ . \quad (19)$$

The solution of this equation has been treated in detail in Ref. [20].

We are interested in the radial intensity distribution $I_S(z,r)$ of the Stokes light

$$I_S(z,r)=\frac{c}{2\pi}\langle \hat{E}^{(-)}(z,\vec{r})\hat{E}^{(+)}(z,\vec{r})\rangle$$
$$=\frac{c}{2\pi}\sum_{n,j,m,l}\langle \hat{a}_n^{l\dagger}\hat{a}_m^j\rangle\phi_m^{j*}\phi_n^l \quad (20)$$

and the Stokes power

$$P_S=2\pi\int_0^{\infty} I_S(z,r)r\,dr \ . \quad (21)$$

The spontaneous polarization correlation function

$$\langle \hat{P}_{\rm sp}^{\dagger}(z,\vec{r})\hat{P}_{\rm sp}(z',\vec{r}')\rangle=\frac{\hbar\delta\nu_R}{2\pi k_S}g(z,r)\delta(z-z')\delta(\vec{r}-\vec{r}') \quad (22)$$

is used for the calculation of the correlation function $\langle \hat{a}_n^{l\dagger}\hat{a}_m^j\rangle$ in Eq. (20). $\delta\nu_R$ is the Raman linewidth [full width at half maximum (FWHM)]. It is presupposed that the population of the vibrational ground state of the molecule is not changed by stimulated Raman scattering.

From the solutions of the Eqs. (11), (12), and (19) we calculate the Raman Stokes intensity

$$I_S(r)=\hbar\omega_S\delta\nu_R\sum_{n,m,l}B_{n,m}^l\{\exp[(\lambda_n^l+\lambda_m^{l*})\theta_t]-1\}$$
$$\times\phi_m^{l*}(\theta_{\rm ex},r)\phi_n^l(\theta_{\rm ex},r) \quad (23)$$

and the Stokes power

$$P_S(\theta_t)=\hbar\omega_S\delta\nu_R\sum_{n,m,l}(B_{n,m}^l)^2\{\exp[\lambda_n^l+\lambda_m^{l*})\theta_t]-1\} \ . \quad (24)$$

The value of the propagation parameter $\theta_t=\theta_{\rm ex}-\theta_{\rm en}$ is obtained from Eq. (9) at the entrance ($z=\ell_{\rm en}$) and exit ($z=\ell_{\rm ex}=\ell_{\rm en}+\ell$) of the Raman medium:

$$\theta_t=\tan^{-1}[(\ell_{\rm en}+\ell)/z_0]-\tan^{-1}(\ell_{\rm en}/z_0) \ . \quad (25)$$

It is interesting to consider the special case that the output is dominated by the lowest-order *nonorthogonal* Stokes mode ϕ_0^0. Then the Stokes power is given by

$$P_S\approx\hbar\omega_S\delta\nu_R(B_{0,0}^0)^2\{\exp[2\,{\rm Re}(\lambda_0^0)\theta_t]-1\} \ . \quad (26)$$

In the *low-gain* regime the eigenvalue of this mode is

$$2\,{\rm Re}(\lambda_0^0)=\mu G_{Rr} \ . \quad (27)$$

The results of Eqs. (23)–(27) will be compared with the results of the adapted plane-wave theories in Sec. IV. In order to account approximately for spectral narrowing of the Stokes light, the Raman linewidth $\delta\nu_R$ will be replaced by $\delta\nu_R/(\mu G_{Rr}\theta_t+1)^{1/2}$ in Eqs. (23) and (24) [20].

B. Numerical results

1. Raman gain

We calculated first the eigenvalues λ_n^l, which determine the Raman gain, by solving the coupled equations (11). It can be seen from Eq. (11) that the eigenvalues depend only on the mode filling factor μ and the Rayleigh range gain G_{Rr}. Equation (14) shows that G_{Rr} is proportional to the laser power P_L, but it is independent of the Rayleigh range z_0. This means that for an unfocused beam and for beams focused with different focal lengths the same eigenvalues λ_n^l are obtained for a definite laser power (with wave vector $\vec{k}_L$) in a specific Raman medium.

The calculations were carried out for SRS in H_2 gas (Raman shift 4155 cm^{-1}) with the second harmonic of the Nd:YAG laser, $k_L=118\,105$ cm^{-1} and $\mu=0.4379$ [from Eq. (15)]. We used a Raman gain factor of $g_0=2.6\times10^{-3}$ cm/MW (at 532 nm) and a spontaneous Raman linewidth of $\delta\nu_R=4.6\times10^9$ s^{-1} (at 100 bar). The equations were usually solved for $n,p'=0,1,\ldots,40$ and $l=0,1,\ldots,6$. Figure 1 shows as an example the normalized real parts of the eigenvalues λ_n^0 as a function of the Rayleigh range gain G_{Rr} (lower scale). On the upper scale the laser power P_L is plotted. It should be emphasized that all eigenvalues depend *nonlinearly* on G_{Rr}, i.e., on the laser power P_L. This is in contrast to the linear dependence obtained in the plane-wave theory (see Sec. III).

The following details are of interest.

(i) Lowest-order nonorthogonal mode ($n=l=0$). For low laser power $P_L<0.1$ MW, the real part of the eigenvalue is given by $2\,{\rm Re}(\lambda_0^0)=\mu G_{Rr}$ (see Fig. 1). In this region the main contribution to ϕ_0^0 comes from the lowest-order free-space Stokes mode U_0^0, which has about the

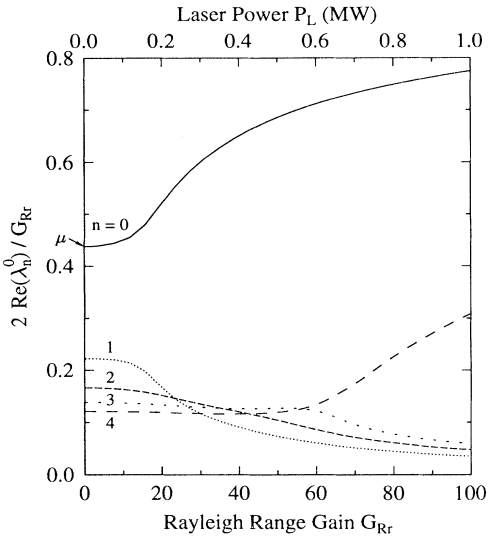

FIG. 1. Normalized real part $2\,\mathrm{Re}(\lambda_n^0)/G_{Rr}$ of the eigenvalues of Eq. (11) versus the Rayleigh range gain G_{Rr} (lower scale) and the laser power P_L (upper scale).

same diameter as the laser beam. The overlap of the laser and the Stokes beams is responsible for the mode filling factor μ in the real part of the eigenvalue λ_0^0. For very high laser power $P_L \gg 1$ MW, we get $2\,\mathrm{Re}(\lambda_0^0) \approx G_{Rr}$, because the Stokes beam radius is much smaller than the laser beam radius (see Fig. 4, $\theta_t = 0.1$) and the Stokes light is amplified by the peak intensity in the center of the laser beam.

(ii) Higher-order nonorthogonal modes. The eigenvalues of these modes are close together for low laser power, i.e., all these modes are important for the calculation of the Stokes power.

2. Raman Stokes power

It can be seen from Eq. (24) that the important parameters entering the Stokes power P_S are the factors $(B_{n,m}^l)^2$, which are a measure of the overlap between the nonorthogonal modes, and the product of the eigenvalues λ_n^l with the propagation parameter θ_t. θ_t is equal to the difference of the propagation parameters at the exit and entrance of the Raman medium. It depends on the position of the Raman cell (entrance $z = \ell_{\mathrm{en}}$), its length ℓ (exit $z = \ell_{\mathrm{ex}} = \ell_{\mathrm{en}} + \ell$) and the Rayleigh range z_0 [Eq. (25)], which is determined by the focal length f of the focusing lens. For a singlepass cell, the maximum value of θ_t is π. For a multipass cell, Battle and co-workers [20] have shown that θ_t can be much larger than π, depending on the number of passages of the laser beam through the Raman cell.

We have calculated the Raman Stokes power P_S for three cases.

(i) The Raman cell is short compared to the Rayleigh range ($\ell \ll z_0$) or far away from the focal region ($\ell_{\mathrm{en}} \gg z_0$). In this case θ_t is small. We used a value of $\theta_t = 0.1$ in the calculations, which can be realized experimentally in different ways. For example, for an unfocused laser beam with $z_0 = 500$ cm and a long cell length $\ell = 824$ cm far from the beam waist ($\ell_{\mathrm{en}} = 1594$ cm), or a tightly focused laser beam ($z_0 = 5$ cm) and a short cell ($\ell = 3.2$ cm) at $\ell_{\mathrm{en}} = 10$ cm, a value of $\theta_t = 0.1$ is obtained from Eq. (25).

(ii) A Raman cell, which is longer than z_0, is in the focal region of a tightly focused laser beam. In this case, we get $\theta_t \approx \pi$.

(iii) A multipass Raman cell is in the focal region, having enough passages to get a value of $\theta_t = 30$.

In all calculations of the Stokes power P_S the Raman linewidth $\delta\nu_R$ in Eq. (24) has been replaced by $\delta\nu_R/(G+1)^{1/2}$ to account approximately for spectral narrowing of the Stokes light [20]. The results of our calculations of the Stokes power are shown in Fig. 2. The Stokes power P_S is plotted on a logarithmic scale versus the Raman gain $G = \mu g_0 I_L(0,0) z_0 \theta_t = \mu G_{Rr} \theta_t$. We have chosen this expression for the gain because the calculations have shown that in the stimulated scattering regime, often the lowest-order Stokes mode dominates. In the low gain case the exponent in the expression of the Stokes power P_S [Eq. (26)] is then $2\,\mathrm{Re}(\lambda_0^0)\theta_t = G$, using Eqs. (13) and (27). Figure 2(a) shows three solid lines for $\theta_t = 0.1$, π, and 30 calculated according to the nonorthogonal mode theory [Eq. (24)] and a dashed and a dash-dotted line calculated with the one-mode theory and

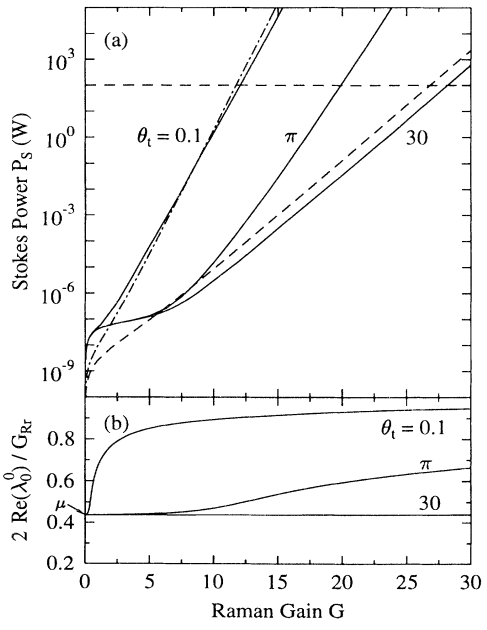

FIG. 2. (a) Logarithm of the Stokes power P_S versus Raman gain G. The solid, the dashed, and the dash-dotted lines were calculated according to the nonorthogonal mode theory, the one-mode theory, and the adapted plane-wave theory, respectively. (b) Normalized real part of the eigenvalue λ_0^0 versus Raman gain G.

the adapted plane-wave theory, respectively, which will be discussed in Sec. IV. It should be noted that the determining quantity for the gain dependence of the Stokes power is the propagation parameter θ_t. The details of the focusing conditions and the position and length of the Raman cell enter only through the value of θ_t.

Figure 2(b) shows the normalized eigenvalue $2\,\mathrm{Re}(\lambda_0^0)/G_{Rr}$ versus Raman gain G. The normalized eigenvalues do not depend on the propagation parameter θ_t, but we get different curves for the three values of θ_t because the Raman gain G, which is plotted on the abscissa, is proportional to θ_t.

Next we discuss the slopes of the three curves for the Stokes power in Fig. 2(a) in the region of nearly exponential growth ($G>7$). In this region the lowest-order nonorthogonal mode dominates and the slope $S_G=d(\log_{10}P_S)/dG$ is calculated from Eq. (26). We get

$$S_G=\frac{1}{\mu}\log_{10}(e)\left[\frac{2\,\mathrm{Re}(\lambda_0^0)}{G_{Rr}}\right], \tag{28}$$

where $\log_{10}(e)$ is the common logarithm of the number $e=2.71828$. We have expressed S_G in terms of the normalized eigenvalue $2\,\mathrm{Re}(\lambda_0^0)/G_{Rr}$, which is plotted in Fig. 2(b) versus G. For $\theta_t=0.1$ the normalized eigenvalue has a high value almost over the complete range of G. Therefore, the Stokes power P_S exhibits the steepest rise [Eq. (28)]. In contrast, $2\,\mathrm{Re}(\lambda_0^0)/G_{Rr}$ stays at its lowest value μ over the whole gain regime for $\theta_t=30$ [Fig. 2(b)]. This means that the slope of the corresponding Stokes power is low [Fig. 2(a)]. The curve for $\theta_t=\pi$ lies in between.

The different gain dependence of the real part of the eigenvalue λ_0^0 in Fig. 2(b) can be understood from the radial intensity distributions of the laser and Stokes beams, which are shown in Fig. 4 for large gain ($G>13$). For $\theta_t=0.1$ (inside solid line) the Stokes beam diameter is much smaller than the laser beam diameter (dotted line). Therefore, the Stokes beam is amplified almost completely with the peak intensity in the center of the laser beam, corresponding to a large value of the real part of the eigenvalue $2\,\mathrm{Re}(\lambda_0^0)\approx G_{Rr}$ [see Fig. 2(b)]. For $\theta_t=30$ (outside solid line in Fig. 4) the Stokes beam diameter is of the order of the laser beam diameter (dotted line in Fig. 4). This leads to a smaller overall amplification, which is determined by the mode filling factor μ. In this case, a smaller value of the real part of the eigenvalue is obtained $2\,\mathrm{Re}(\lambda_0^0)\approx\mu G_{Rr}$ [see Fig. 2(b)]. These examples show that the overlap of the laser and the Stokes beams is relevant for the real parts of the eigenvalues that enter the Raman amplification.

For a comparison with the experiments it is interesting to plot the Stokes power $\log_{10}(P_S)$ versus the laser power P_L [see Fig. 3(a)]. In this case the slope S_P is given by

$$S_P=\frac{\log_{10}(e)}{\pi}k_L g_0\left[\frac{2\,\mathrm{Re}(\lambda_0^0)}{G_{Rr}}\theta_t\right]. \tag{29}$$

The important difference to Eq. (28) is that the slope S_P in Fig. 3(a) is proportional to the normalized eigenvalue $2\,\mathrm{Re}(\lambda_0^0)/G_{Rr}$ times θ_t. As a consequence, the slope for $\theta_t=0.1$ is the smallest, although $2\,\mathrm{Re}(\lambda_0^0)/G_{Rr}$ has almost its full value [Fig. 3(b)]. The slope for $\theta_t=30$ is large [Fig. 3(a)] because θ_t is large [Eq. (29)]. These results can also be understood from the following qualitative considerations. For $\theta_t=30$ the multipass Raman cell is in the focal region with high laser intensity, therefore a low laser power is needed for high amplification. In contrast, the singlepass Raman cell is far from the focus for $\theta_t=0.1$. Far from the focus the laser beam diameter is large, therefore a high laser power is required to get sufficient laser intensity to generate intense Raman light.

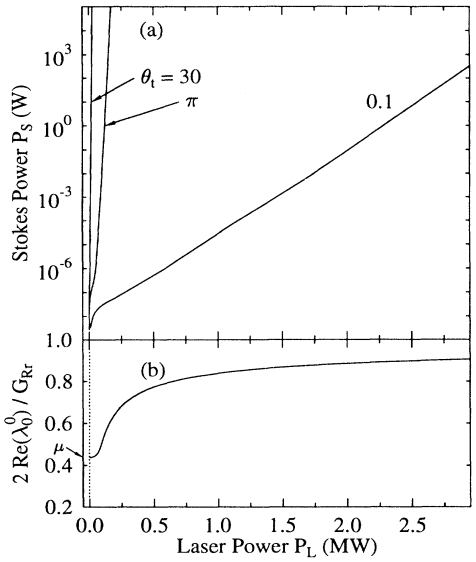

FIG. 3. (a) Logarithm of the Stokes power P_S versus laser power P_L, calculated according to the nonorthogonal mode theory. (b) Normalized real part of the eigenvalue λ_0^0 versus laser power P_L.

3. *Radial intensity distribution of the Stokes beam*

We have calculated the Raman Stokes intensity $I_S(r)$ according to Eq. (23) for different values of the propagation parameter θ_t, which determines the exponential amplification of the modes together with their eigenvalues λ_n^l. The radial intensity distribution depends on the radial distribution of the modes $\phi_n^l(\theta_{ex},r)$ at the exit of the Raman medium. The Stokes intensity $I_S(r)$ was calculated for $\theta_{ex}=1.5$ and $\theta_t=0.1$, π, and 30 using gain values of $G=14$, 20, and 26, respectively, which correspond to a Stokes power of about 100 W [dashed horizontal line in Fig. 2(a)].

Figure 4 shows the normalized Stokes intensity $I_S(r)/I_S(0)$ versus the normalized radial coordinate $r/r_0(\ell_{ex})$. The solid lines correspond to the results of the nonorthogonal mode theory for $\theta_t=0.1$, π, and 30. The dashed, the dash-dotted, and the dotted lines represent the Stokes intensity distributions of the one-mode theory, the adapted plane-wave theory (see Sec. IV) and the laser intensity distribution, respectively. The half-width of the Stokes beam is smaller for smaller values of θ_t. Gain narrowing of the Stokes beam is observed for $\theta_t=0.1$ and π.

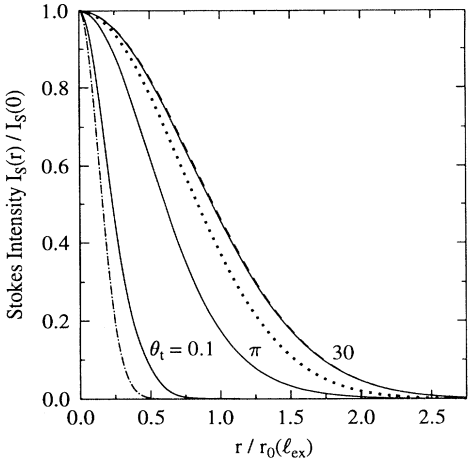

FIG. 4. Normalized Stokes intensity distribution $I_S(r)/I_S(0)$ versus normalized radial coordinate $r/r_0(\ell_{ex})$. The solid, the dashed, and the dash-dotted lines were calculated according to the nonorthogonal mode theory, the one-mode theory, and the adapted plane-wave theory, respectively. The dotted line corresponds to the normalized radial intensity distribution of the laser beam.

The numerical calculations show that for the gain values used in the calculations above the lowest-order nonorthogonal mode ϕ_0^0 dominates. The nonorthogonal modes have been expanded in terms of the free-space modes U_p^l [see Eq. (8)]. The absolute values $|b_{0,p}^0|$ of the expansion coefficients of the ϕ_0^0 mode are presented in Fig. 5 for the indices $p=0-19$. For $\theta_t=0.1$ many free-space modes contribute to the ϕ_0^0 mode [Fig. 5(a)]. The superposition of these modes leads to the narrow width of the Stokes intensity shown in Fig. 4 (inside solid line). For $\theta_t=30$ the lowest-order free-space mode U_0^0 dominates [Fig. 5(b)], causing the large half-width of the Stokes intensity in Fig. 4 (outside solid line).

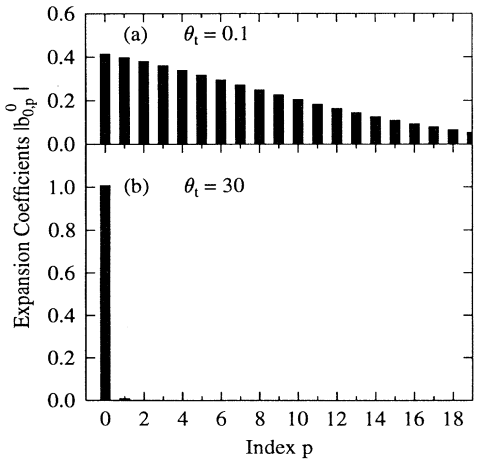

FIG. 5. Expansion coefficients $|b_{0,p}^0|$ of the lowest-order nonorthogonal mode ϕ_0^0 versus the index p. (a) Propagation parameter $\theta_t=0.1$; (b) $\theta_t=30$.

We have also calculated the radial intensity distribution of the Stokes beam for lower values of the Stokes power. Since in these cases the Raman gain is lower, the widths of the Stokes beams are larger than for higher Stokes power. At sufficiently low Stokes power the higher-order nonorthogonal modes become more important and contribute to the increasing width of the Stokes beam.

III. PLANE-WAVE THEORY

Stimulated Raman scattering is usually treated using a plane-wave theory [1–4]. In the plane-wave approximation the transverse variation of the Stokes field [∇_T^2 in Eq. (2)] is neglected compared to the axial variation. The Stokes intensity is then given by [5]

$$I_S=\tfrac{1}{2}\hbar\omega_S\pi A^{-1}F^2\delta\nu_R G_{\mathrm{PW}} \times[I_0(G_{\mathrm{PW}}/2)-I_1(G_{\mathrm{PW}}/2)]\exp(G_{\mathrm{PW}}/2)\ . \quad (30)$$

Here F is the Fresnel number defined as $A/\lambda_S\ell$. A and ℓ are the beam area and cell length, respectively. I_0 and I_1 are the modified Bessel functions. For true plane waves the Raman gain is given by

$$G_{\mathrm{PW}}=g_0 I_L^{(\mathrm{PW})}\ell\ , \quad (31)$$

where $I_L^{(\mathrm{PW})}$ is the intensity of the plane wave. For high Raman gain $G_{\mathrm{PW}}\gg 1$, the Stokes intensity assumes the well-known form

$$I_S=\tfrac{1}{2}\hbar\omega_S\sqrt{\pi}A^{-1}F^2\frac{\delta\nu_R}{\sqrt{G_{\mathrm{PW}}}}\exp(G_{\mathrm{PW}})\ , \quad (32)$$

i.e., it grows nearly exponentially with the gain G_{PW}.

The problem is to adapt the result of the plane-wave theory to the situation of an unfocused or a focused laser beam with a radial and axial intensity distribution $I_L(z,r)$. For a Gaussian laser beam two possibilities have been treated in the literature [24,25]. In both cases the axial intensity distribution of the Gaussian laser beam can be taken into account by replacing the product $I_L^{(\mathrm{PW})}\ell$ [Eq. (31)] by $I_L(0,0)z_0\theta_t$, which corresponds to the integration of the laser intensity over the cell length.

Both cases differ in the way in which the radial intensity distributions are taken into account.

Case (i) is based on a mode theory, where only the lowest-order free-space Stokes mode U_0^0 is considered [24]. Using this one-mode theory, a scaled plane-wave theory has been given in the literature [20]. The true plane-wave gain G_{PW} in Eqs. (30) and (32) is replaced by the gain $G=\mu g_0 I_L(0,0)z_0\theta_t=\mu G_R\theta_t$ of a single Gaussian Stokes mode. The mode filling factor μ takes into account the overlap of the radial intensity distributions of the laser and the Stokes beams. It should be mentioned that the gain G corresponds to the Raman gain of the lowest-order Stokes mode of the nonorthogonal mode theory in the low gain regime (Sec. II A). The radial Stokes intensity distribution is Gaussian with a $1/e$ radius r_S, which is given by $r_S=r_0\sqrt{k_L/k_S}$, where r_0 is

the $1/e$ radius of the laser beam. The spot size w_S of the Stokes field is related by r_S to $r_S = w_S/\sqrt{2}$. Since $k_L > k_S$ the Stokes beam radius is slightly larger than the laser beam radius. The Stokes power P_S is obtained by multiplying the Stokes intensity I_S [Eq. (30)] with the beam area A.

In case (ii) the radial dependence of the laser intensity is taken into account explicitly [25]. The true plane-wave gain G_{PW} in Eq. (30) is replaced by

$$g_0 I_L(0,0) z_0 \theta_t \exp[-r^2/r_0^2(\ell_{\mathrm{ex}})] = G_{Rr}\theta_t \exp[-r^2/r_0^2(\ell_{\mathrm{ex}})] . \quad (33)$$

The radial intensity distribution of the laser beam determines via Eqs. (30) and (33) the radial intensity distribution of the Stokes beam. When the Gaussian distribution in Eq. (33) is approximated by a parabolic distribution, it can be shown that the ratio of the Stokes beam radius to the laser beam radius is $(G_{Rr}\theta_t)^{-1/2}$. For $G_{Rr}\theta_t = 25$ the Stokes beam radius is $\frac{1}{5}$ of the laser beam radius. The Stokes power P_S is calculated by integrating numerically the Stokes intensity $I_S(r)$ [Eq. (30)] over the Stokes beam cross section.

IV. COMPARISON OF THE NONORTHOGONAL MODE THEORY AND THE ADAPTED PLANE-WAVE THEORIES

Two cases of the plane-wave theory adapted to a Gaussian laser beam have been discussed in the preceding section. When only the lowest-order free-space Stokes mode U_0^0 is considered [24], case (i), the radial Stokes intensity distribution $I_S(r)$ is given by this mode. $I_S(r)$ is shown as a dashed line in Fig. 4, which can hardly be distinguished from the solid line for $\theta_t = 30$. The reason for this good agreement comes from the fact that for $\theta_t = 30$ the lowest-order nonorthogonal mode ϕ_0^0, which dominates, consists mainly of the lowest-order free-space mode U_0^0 [Fig. 5(b)].

The Stokes power for case (i) was calculated introducing the gain $G = \mu g_0 I_L(0,0) z_0 \theta_t$ in Eq. (30) and multiplying with the beam area A. The result is shown in Fig. 2(a) as a dashed line. In the region of stimulated Raman scattering ($G > 7$) there is satisfactory agreement between the slopes of the one-mode theory and the nonorthogonal mode theory for $\theta_t = 30$, which correspond to the multipass cell. This can be understood from Fig. 2(b) where the normalized eigenvalue of the lowest-order Stokes mode is plotted versus G. It can be seen that $2\,\mathrm{Re}(\lambda_0^0)\theta_t \approx \mu G_{Rr}\theta_t = G$. This agrees with the gain of the one-mode theory. The results of the nonorthogonal mode theory for the singlepass cell ($\theta = 0.1$ and π) deviate strongly from the one-mode theory [dashed line in Fig. 2(a)].

In case (ii) [25] the radial intensity distribution of the laser beam [Eq. (33)] has been introduced in Eq. (30). The radial intensity distribution of the Stokes beam depends on the gain $G_{Rr}\theta_t$ [Eq. (33)]. Using the relation $G_{Rr}\theta_t = G/\mu$, we have calculated $I_S(r)$ from Eq. (30) for $G = 14$ and $\theta_t = 0.1$. The result is shown as a dash-dotted line in Fig. 4. The half-width of this curve is only slightly smaller than that of the corresponding inside solid line calculated from the nonorthogonal mode theory for $\theta_t = 0.1$. It shows the typical gain narrowing.

The Stokes power P_S for case (ii) has been calculated as a function of the Raman gain G by introducing Eq. (33) in Eq. (30) and integrating Eq. (30) over the beam cross section. This result is shown as a dash-dotted line in Fig. 2(a). In the region of stimulated Raman scattering ($G > 5$) there is satisfactory agreement between the adapted plane-wave theory (dash-dotted line) and the nonorthogonal mode theory for $\theta_t = 0.1$ (solid line), which corresponds, for example, to a Raman cell far from the focal region. For $G > 5$, the nonorthogonal mode theory yields the result $2\,\mathrm{Re}(\lambda_0^0)\theta_t \approx G_{Rr}\theta_t$ [see Fig. 2(b), $\theta_t = 0.1$], which is equal to the gain of the adapted plane-wave theory [see Eq. (33)] in the center of the laser beam. For small values of θ_t the Rayleigh range gain G_{Rr} must be large to get a definite Stokes power [see, e.g., Eqs. (26) and (27)]. In this case, the axial variation of the Stokes light is large compared to the transverse variation, i.e., the plane-wave theory is a good approximation.

In conclusion, it should be emphasized that the results of the nonorthogonal mode theory are reproduced by a suitable adapted plane-wave theory in a good approximation only for two limiting cases: (i) for very large values of the propagation parameter θ_t the one-mode theory [24] with the gain $G = \mu g_0 I_L(0,0) z_0 \theta_t$ provides good agreement and (ii) for very small values of θ_t the adapted plane-wave theory [25] using Eqs. (30) and (33) is appropriate.

V. SPONTANEOUS RAMAN SCATTERING

In the limit of very low gain, $(\lambda_n^l + \lambda_m^{l*})\theta_t \ll 1$, spontaneous Raman scattering occurs. In this case, several approximations can be made in the calculation of the Stokes power P_S from Eq. (24). The factor $B_{n,m}^l$ can be approximated by 1 and 0 for $n = m$ and $n \neq m$, respectively. The real parts of the eigenvalues can be written as $\mathrm{Re}(\lambda_n^l) = G_{Rr} f_n^l(\mu)$, where $f_n^l(\mu)$ is obtained from the numerical solution of the eigenvalue equation (11) for $G_{Rr} \ll 1$. Using these approximations we get for the Stokes power

$$P_S \approx \frac{2}{\pi} \hbar \omega_S \delta \nu_R k_L g_0 P_L \theta_t \sum_{n,l} f_n^l(\mu) . \quad (34)$$

The dependence of the Raman gain factor g_0 on the number density N of molecules and the spontaneous Raman scattering cross section $d\sigma/d\Omega$ is given in Ref. [26]. It is introduced in Eq. (34) to give the Stokes power

$$P_S \approx N \frac{d\sigma}{d\Omega} \left[\frac{8}{\pi} \frac{\bar{\nu}_L}{\bar{\nu}_S^2} \theta_t \sum_{n,l} f_n^l(\mu) \right] P_L . \quad (35)$$

It is interesting to compare Eq. (35) with the result of the standard calculations for spontaneous Raman scattering. From Ref. [21] we get

$$P_S = \frac{d\sigma}{d\Omega} \Delta\Omega N_{\mathrm{total}} I_L , \quad (36)$$

where N_{total} is the *total number* of molecules illuminated

by the laser beam with the intensity I_L. $\Delta\Omega$ is the solid angle in which the Stokes power P_S is detected. In our case, the laser intensity I_L depends on r and z [see Eqs. (3) and (4)]. We therefore replace the product $N_{\text{total}} I_L$ in Eq. (36) by $N \int I_L(z,r) dV$, where the integral is over the volume V illuminated by the laser beam and N is the number *density* of molecules. Introducing the intensity $I_L(z,r)$ from Eq. (3) into the volume integral and integrating over r and z, we get

$$P_S = N \frac{d\sigma}{d\Omega} [\Delta\Omega \ell] P_L \ , \tag{37}$$

where ℓ is the length of the Raman medium.

Next we compare the results for the Stokes power P_S obtained from both calculations. As expected, in both cases P_S is proportional to the laser power P_L, the number density N of molecules, and the spontaneous Raman scattering cross section $d\sigma/d\Omega$. The results of Eqs. (35) and (37) differ in the terms in the square brackets. In the nonorthogonal mode theory [20] the Stokes power P_S [Eq. (35)] is proportional to the propagation parameter θ_t, which depends on the cell length ℓ, the position of the cell ℓ_{en}, and the Rayleigh range z_0 [Eq. (25)]. In Sec. III we have introduced θ_t in the one-mode theory and the adapted plane-wave theory. In this case, the Stokes power is also proportional to θ_t for these theories. In contrast, the standard calculations of spontaneous Raman scattering [21] yield a Stokes power P_S that is proportional to the solid angle $\Delta\Omega$ and the cell length ℓ [Eq. (37)]. It does not depend on the position of the cell and the focusing conditions. In Sec. VII B both results will be compared with the measurements of spontaneous Raman scattering in H_2 gas.

VI. EXPERIMENTAL SETUP

The experimental setup is shown schematically in Fig. 6. The laser system (Spectron Laser Systems model SL 803) consists of an injection-seeded, single-frequency Nd:YAG laser oscillator and two amplifiers. A telescope after the laser oscillator provides optimum illumination of the amplifier rods and compensates for the thermal lens effect of the amplifier rods. Depending on the adjustment of the telescope lenses, we obtained different values of the laser beam parameters (see Sec. VII A). The Q-switched laser pulse was frequency doubled and had a duration of 12 ns (FWHM) and a power P_L of up to 10 MW. The distance between the Nd:YAG laser system and the polarizer PO1 was about 15 m. The laser power was varied by rotating the optical axis of the half wave plate with respect to the transmission direction of the polarizer PO2. A small part of the laser light was coupled out with a glass plate and detected with a fast photocell (PC) and a transient digitizer (Tektronix SCD 1000). The rise time of the detection system was about 0.5 ns. The detection sensitivity of the photocell was calibrated with an energy meter (company Ophir, model DGX).

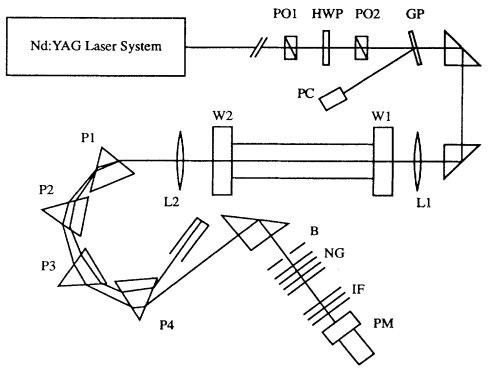

FIG. 6. Schematic diagram of the experimental setup for stimulated Raman scattering in H_2 gas. PO1, PO2, polarizers; HWP, half wave plate; GP, glass plate; PC, photocell; L1, L2, lenses; W1, W2, windows of H_2 cell; P1–P4, prisms; NG, neutral density filters; IF, interference filters; PM, photomultiplier.

The laser beam was focused with lens L1 (focal length $f=350$ cm) into the Raman cell. At a H_2 pressure of 100 bar (density 89 amagat) the damping constant $\Gamma = 2\pi\delta\nu_R$ of the molecular vibrations is 2.9×10^{10} s^{-1} [27,28], i.e., SRS occurs in the steady-state regime for a laser pulse duration of 12 ns. Lens L2 was used to recollimate the laser and the Stokes beam. The laser wavelength ($\lambda_L = 532$ nm) was separated from the Stokes wavelength ($\lambda_S = 683$ nm) by four prisms P1–P4 and suitable narrow-band interference filters in front of the photomultiplier (PM) (Hamamatsu R928), which detected the Stokes energy. In the early experiments the distance between the exit window W2 and the PM was large (400 cm). Later it was reduced to 127 cm in order to get a larger solid angle, which is important for the spontaneous Raman measurements.

The output of the PM was connected to an analog-to-digital converter followed by a computer and was simultaneously observed on the screen of an oscilloscope. In order to measure in the linear range of the photomultiplier, the Raman Stokes pulse was attenuated by suitable neutral density filters. The detection sensitivity of the photomultiplier was calibrated using an energy meter and neutral density filters with known transmission values.

VII. EXPERIMENTAL RESULTS AND DISCUSSION

We have investigated Raman scattering in H_2 gas from the spontaneous to the stimulated scattering regime. For the comparison of the experimental results with the calculations based on the nonorthogonal mode theory and the adapted plane-wave theories the laser beam parameters have been determined for the unfocused and the focused laser beam.

A. Laser beam parameters

We have measured the radial intensity distribution of the laser beam over a wide range of distances from the laser system using a beam analyzing system (Big Sky Laser Technologies, Inc., Beam View Analyzer PC V3.0B). The measured intensity distributions were close

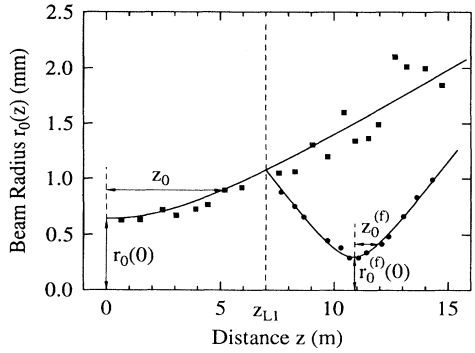

FIG. 7. Measured beam radius $r_0(z)$ of the unfocused (squares) and the focused (circles) laser beams versus the distance z from the beam waist of the unfocused beam. The solid lines represent the fits to the experimental points using Eq. (4). z_0 and $r_0(0)$ are the Rayleigh range and the $1/e$ radius of the laser intensity distribution in the beam waist, respectively. The superscript (f) is used for the values of the focused beam. z_{L1} is the position of lens L1.

to Gaussian distributions. From the fit of a Gaussian curve to the measured distribution we obtained the $1/e$ radius $r_0(z)$ of the laser intensity distribution. Figure 7 shows an example of the beam radius $r_0(z)$ as a function of the distance z from the beam waist ($z=0$) of the unfocused laser beam. The squares and the circles represent the experimental points for the unfocused and the focused beam (lens L1 at z_{L1}, focal length $f=350$ cm), respectively. The solid lines have been fitted to the experimental points using Eqs. (4) and (5).

From the fit we obtained the relevant parameters of the laser beam, i.e., the radius $r_0(0)$ in the beam waist and the Rayleigh range z_0. In Fig. 7 the superscript (f) is used for the focused beam. The measured numbers are given in Table I for the unfocused and the focused beam. Depending on the adjustment of the telescope between the laser oscillator and the amplifiers, the thermal lens of the amplifier rods is compensated in a different way. This is the origin of the differences in the beam radii $r_0(0)$ and the Rayleigh ranges z_0 for configurations I and II, which are shown as typical examples in Table I. The ratio $z_0/r_0^2(0)$ is always close to the value of the laser wave vector $k_L=118\,105$ cm^{-1}, as expected for a diffraction limited beam [Eq. (5)]. The value of z_0 is needed for determining the propagation parameter θ_t [Eq. (25)], which enters the calculation of the Stokes power P_S [Eq. (24)].

TABLE I. Beam parameters for the unfocused and the focused laser beams with two adjustments of the telescope between the laser oscillator and the amplifiers. $r_0(0)$ is the $1/e$ radius of the laser intensity in the beam waist, z_0 is the Rayleigh range, and $f=350$ cm is the focal length of the lens.

Focusing conditions	Telescope configuration I unfocused	I focused	II unfocused	II focused
$r_0(0)$ (mm)	1.01	0.19	0.65	0.30
z_0 (cm)	1235	44	509	112
$\frac{z_0}{r_0^2(0)}$ (cm^{-1})	121 067	121 884	120 473	124 444

B. Spontaneous Raman scattering

Before we discuss our measurements of spontaneous Raman scattering in H_2 gas with the Q-switched Nd:YAG laser, we consider two experimental details that influence the measured spontaneous Stokes power and should be taken into account in an accurate comparison between experiments and calculations.

(i) The photomultiplier detects the sum of the $Q(0)$–$Q(4)$ lines because the bandwidth of the interference filters (see Fig. 6) is broad (FWHM about 215 cm^{-1}). The Q lines with higher rotational quantum numbers are very weak and can be neglected. We calculated the ratio of the total spontaneous Raman energy to the energy of the $Q(1)$ line to be 1.5. This factor was taken into account in the spontaneous Raman measurements.

(ii) The off-axis scattered spontaneous Raman light is reflected from the walls of the Raman cell, which was made from brass. Part of the reflected Raman light is detected by the photomultiplier and contributes to the measured Raman energy. Since it is difficult to calculate the contribution of the reflected Raman light, we used for a quantitative comparison between the calculations and the measurements only experimental configurations where the reflected light can be neglected. It can be shown that this is the case if the distance d_{PM} between the exit window W2 of the cell and the photomultiplier (see Fig. 6) is larger than the cell length ℓ. In this estimate it has been taken into account that the diameter of the sensitive area of the photomultiplier and the inner diameter of the Raman cell are approximately equal.

When the experimental setup of Fig. 6 was used in the spontaneous Raman measurements the detection threshold was limited to about 4×10^{-16} J of Stokes energy by stray and fluorescence light. We reduced the disturbing light by approximately a factor of 4 by introducing two filters, which reflect more than 99% of the green laser light, after the exit window W2. The improvement has been confirmed by measuring the photomultiplier signal after the H_2 gas was pumped off. With this improved setup we have measured the spontaneous Raman Stokes energy E_S in H_2 gas at 100 bar and 300 K for different experimental conditions. We used Raman cells with lengths $\ell=108$ and 409 cm at distances d_{PM} between the exit window W2 and the photomultipler larger than the respective cell lengths to avoid contributions of reflections from the cell walls to the spontaneous Raman energy. We have carried out measurements with different distances d_{PM} between W2 and the PM because d_{PM} determines the solid angle $\Delta\Omega$ that enters the standard theory of spontaneous Raman scattering. In addition, the focusing conditions, which influence the propagation parameter θ_t of the nonorthogonal mode theory, were changed. Figure 8 shows the measured Stokes energy E_S

versus peak power P_L of the laser pulse in a double-logarithmic plot. Each experimental point represents an average over 100 shots at a particular pump laser power ($\pm 2\%$).

The results in Fig. 8(a) were obtained for a cell length of $\ell = 108$ cm. The open and the solid circles correspond to a distance $d_{PM} = 297$ cm for the unfocused and the focused ($f = 350$ cm) laser beam, respectively. The squares were measured with the focused laser beam, but for a much shorter distance between exit window W2 and the photomultiplier ($d_{PM} = 127$ cm). Figure 8(b) shows the results for a 409-cm-long cell at a distance $d_{PM} = 543$ cm for a focused laser beam.

We have compared the experimental results with calculations based on the nonorthogonal mode theory and the standard theory of spontaneous Raman scattering. The solid lines in Fig. 8 were calculated by integrating Eq. (24) for the Stokes power P_S numerically over the pulse duration to obtain the Stokes energy E_S from the nonorthogonal mode theory. In the spontaneous scattering region the calculated Stokes power P_S depends on the number of modes taken into account in the numerical calculations. Therefore, in the comparison between calculations and experiments special emphasis was given to the dependence of the Stokes power P_S on the propagation parameter θ_t, not to the absolute values of P_S. We used in the calculations the values of the propagation parameter θ_t given in Table II, where all numbers relevant for the measurements of Fig. 8 are given.

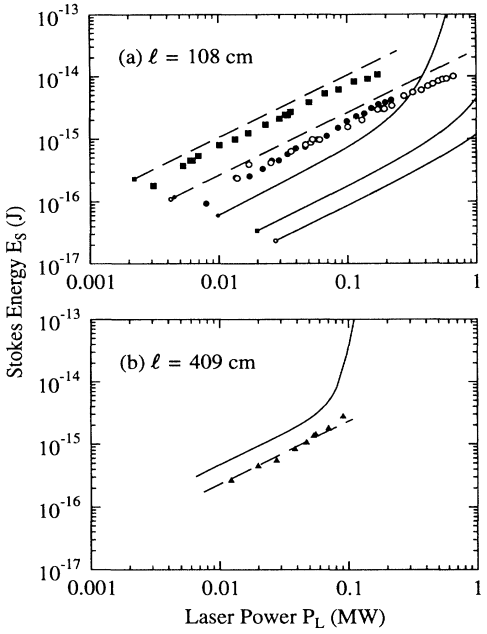

FIG. 8. Double-logarithmic plot of the Stokes energy E_S versus the laser power P_L in the spontaneous scattering region. The solid and the dashed lines were calculated according to the nonorthogonal mode theory and the standard theory of spontaneous Raman scattering, respectively. For an easy identification the calculated curves are marked at the left end with the symbol corresponding to the experimental points. (a) Cell length $\ell = 108$ cm. The open and the closed circles represent the experimental points of the unfocused and the focused laser beam, respectively, with a distance of $d_{PM} = 297$ cm between the exit window W2 of the Raman cell and the photomultiplier PM. The closed squares correspond to $d_{PM} = 127$ cm (focused laser beam). (b) Cell length $\ell = 409$ cm. The closed triangles represent the experimental points for $d_{PM} = 543$ cm (focused beam).

As an example we consider the open and the solid circles in Fig. 8(a), which correspond to the unfocused and the focused beam, respectively, and therefore to completely different values of θ_t. The measured points lie on the same straight line within the experimental accuracy, while the nonorthogonal mode theory (solid lines) predicts a large difference between the unfocused and the focused beam. For an easy identification of the calculated curves we have marked the solid lines at the left end with the symbol of the corresponding experimental points. Likewise the other results in Fig. 8 show that the nonorthogonal mode theory does not describe the spontaneous Raman measurements correctly. We think that the following reasons are responsible for the disagreement between the measurements and the nonorthogonal mode theory. In the nonorthogonal mode theory the paraxial approximation has been used, which is a good approximation for collimated light beams [29] as they occur, e.g., for SRS. It is not valid for spontaneous Raman scattering, where the Stokes light is scattered in all directions. In addition, the use of a Gaussian laser beam leads to the introduction of the propagation parameter θ_t, which enters the exponent of the amplification term [see Eq. (24)]. The expansion of the Stokes power for small gain results in the proportionality to θ_t [Eq. (34)], in disagreement with the experiment.

We have calculated the spontaneous Stokes energy E_S from the standard theory of spontaneous Raman scattering [Eq. (37)]. The solid angle $\Delta\Omega$, in which the Stokes energy is detected, has been replaced by an effective solid angle $\Delta\Omega_{eff}$ because Raman light from all parts of the Raman cell is collected by the photomultiplier. In the spontaneous Raman measurements described above, the lens L2 after the Raman cell (see Fig. 6) was removed. In this case, the effective solid angle can be calculated in the following way:

$$\Delta\Omega_{eff} = \frac{F_{PM}}{\ell}\int_0^{\ell}\frac{dz}{[\ell + d_{PM} - z]^2} = \frac{F_{PM}}{\ell}\left[\frac{1}{d_{PM}} - \frac{1}{\ell + d_{PM}}\right]. \quad (38)$$

Here F_{PM} and d_{PM} are the sensitive area and the distance of the photomultiplier from the exit window W2 of the Raman cell, respectively, and ℓ is the cell length. The values used in the calculations of the spontaneous Raman Stokes energy from Eq. (37) are given in Table II. At a H_2 pressure of 100 bar (89 amagat) the number density of molecules in the $J = 1$ state is $N_1 = 1.54 \times 10^{21}$ cm^{-3}.

TABLE II. Numerical data for the calculations of spontaneous Raman scattering. ℓ is the cell length, ℓ_{en} is the distance of the entrance window W1 from the position of the beam waist, z_0 is the Rayleigh range, θ_t is the propagation parameter, d_{PM} is the distance of the photomultiplier to the exit window W2, $\Delta\Omega_{eff}$ is the effective solid angle, and $F_{PM}=2$ cm^2 is the sensitive area of the photomultiplier.

Focusing conditions	ℓ (cm)	ℓ_{en} (cm)	z_0 (cm)	θ_t	d_{PM} (cm)	$\Delta\Omega_{eff}$ (10^{-6} sr)	Symbol in Fig. 8
unfocused	108	2610	1970	0.02	297	16	○
focused	108	130	48	0.15	297	16	●
$f=350$ cm	108	300	48	0.04	127	64	■
	409	−416	48	1.31	543	3.7	▲

The spontaneous Raman scattering cross section at the pump wavelength of 532 nm is $d\sigma/d\Omega=8.0\times10^{-31}$ cm^2/sr [30,31]. The results of the calculations are shown in Fig. 8 as dashed lines. Considering the limited accuracy of the calibration of the measured Stokes energy and of the calculation of the effective solid angle, the standard theory of spontaneous Raman scattering is in good agreement with the experimental results. It predicts correctly the dependence of the measured Raman energy on solid angle [Fig. 8(a)] and cell length [Fig. 8(b)]. In particular, in Fig. 8(a) there is no deviation between the open and the solid circles, which correspond to the same solid angle but to different values of θ_t.

From the results discussed above we conclude that the nonorthogonal mode theory does not describe correctly the spontaneous Raman scattering regime. Therefore, the calculated results for the transition region between spontaneous and stimulated Raman scattering should also be considered with caution.

C. Stimulated Raman scattering

We have estimated the Raman gain factors of the $Q(J)$ lines ($J=0,1,\ldots,4$) from the number densities N_J, the Raman scattering cross section $d\sigma/d\Omega$, and the spontaneous Raman linewidths $(\delta\nu_R)_J$ [28]. We found that in the stimulated scattering region it is sufficient to take into account the $Q(1)$ Raman line because the Raman gain factors of the other Q lines are smaller by at least a factor of 8. We used a Raman gain factor $g_0=2.6\times10^{-3}$ cm/MW (for $\lambda_L=532$ nm) [32] and a Raman linewidth $\delta\nu_R=4.6\times10^9$ s^{-1} [27,28] for the $Q(1)$ line at a H_2 gas pressure of 100 bar (density 89 amagat).

Recent investigations of SRS in H_2 gas [14] have shown that for a Raman cell shorter than the length of the laser pulse, the experimental results are influenced by feedback from diffuse reflections of the cell windows and of optical elements outside the H_2 cell. Therefore, we tested our calculations of SRS (Sec. II and III) by a comparison with measurements using a cell ($\ell=824$ cm) longer than the pulse length (360 cm).

The determining quantity in the nonorthogonal mode theory is the propagation parameter θ_t [Eq. (25)]. In the experiments we have selected two completely different values of θ_t by measuring with the unfocused ($\theta_t=0.3$) and the focused ($\theta_t=2.7$) laser beam. In Fig. 9 the measured Stokes energy E_S is plotted on a logarithmic scale versus the laser power P_L for the unfocused and the focused laser beam, represented by the open and the closed circles, respectively. Since for the focused beam the laser intensity is higher than for the unfocused beam, much less laser power is needed to generate the same Stokes power (see Fig. 9).

We have compared the experimental results with the results of the nonorthogonal mode theory (Sec. II), the one-mode theory, and the adapted plane-wave theory (Sec. III). The solid lines in Fig. 9 were calculated by integrating Eq. (24) numerically over the pulse duration to obtain the Stokes energy E_S of the nonorthogonal mode theory. Spectral narrowing of the Stokes light was taken into account in the same way as in Sec. II B2. The calculated solid lines of the nonorthogonal mode theory are in good agreement with the experimental points in the region of stimulated Raman scattering ($P_L>0.08$ and 0.4 MW for the focused and the unfocused beam, respective-

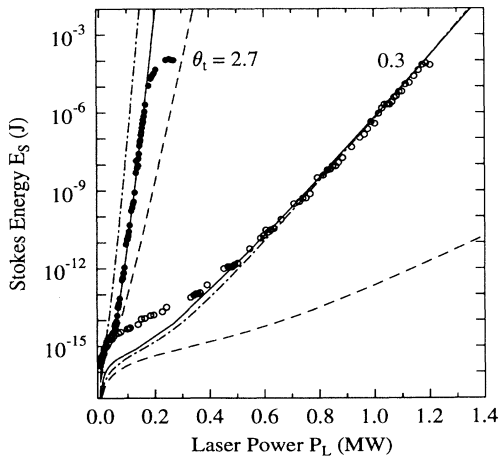

FIG. 9. Logarithm of the Stokes energy E_S versus laser power P_L. The closed and the open circles represent the experimental points for the focused and the unfocused laser beam, respectively. The solid, the dashed, and the dash-dotted lines were calculated according to the nonorthogonal mode theory, the one-mode theory, and the adapted plane-wave theory, respectively.

ly). The sensitive dependence of the experimental results on the propagation parameter θ_t is described correctly by the nonorthogonal mode theory. The deviations between the measured points and the curves calculated from the nonorthogonal mode theory in the spontaneous scattering regime have been discussed in Sec. VII B. It can be seen from Fig. 9 ($\theta_t=0.3$) that also the one-mode theory (dashed line) and the adapted plane-wave theory (dash-dotted line) fail to describe the measurements in this regime.

The results of the one-mode theory and the adapted plane-wave theory are shown in Fig. 9 as dashed and dash-dotted lines, respectively. In the one-mode theory the plane-wave gain G_{PW} in Eq. (30) was replaced by the single-mode gain G. Equation (30) was multiplied by the beam area A and integrated over time to obtain the Stokes energy E_S. In the adapted plane-wave theory $g_0 I_L(0,0,t) z_0 \theta_t \exp[-r^2/r_0^2(\ell_{\mathrm{ex}})]$ [see Eq. (33)] was introduced in Eq. (30). E_S was calculated by integrating Eq. (30) numerically over the beam cross section and time, assuming a Gaussian time dependence of the laser intensity. For the focused beam the experimental points (closed circles in Fig. 9) are in between the calculated dashed and dash-dotted curves. They do not agree with either of these curves as expected from the results of Sec. IV for a value of $\theta_t=2.7$. For the unfocused beam ($\theta_t=0.3$) the experimental points (open circles) are in good agreement with the dash-dotted curve of the adapted plane-wave theory. For small values of θ_t the Rayleigh range gain G_{Rr} must be large to get a definite Stokes power [see, e.g., Eqs. (26) and (27)]. In this case, the axial variation of the Stokes light is large compared to the transverse variation, i.e., the plane-wave theory is a good approximation.

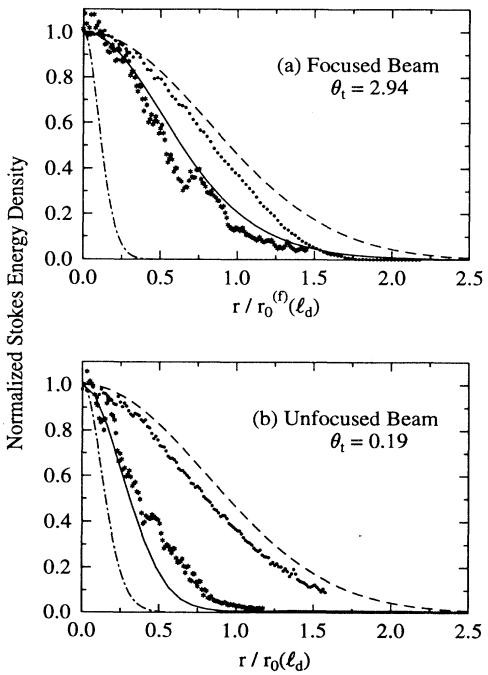

FIG. 10. Normalized Stokes energy density versus normalized radial coordinate $r/r_0(\ell_d)$, where ℓ_d corresponds to the position of the detection system. (a) Focused and (b) unfocused laser beam. The stars and the points correspond to the measured Stokes and the laser beam, respectively. The solid, the dashed, and the dash-dotted lines were calculated according to the nonorthogonal mode theory, the one-mode theory, and the adapted plane-wave theory, respectively.

We have measured the radial energy density distributions of the Stokes and the laser beam close to the end of the H_2 cell (distance from the exit window W2 about 20 cm). The results are shown for the focused and the unfocused laser beam in Figs. 10(a) and 10(b), respectively. The stars and the points correspond to the measured Stokes and the laser energy density distributions, respectively. They represent an average over 100 shots with about the same Stokes and laser power. The experimental points exhibit a slight periodic modulation because of interference effects from optical elements. The lines have been calculated. It can be seen in Fig. 10(a) that the Stokes beam (stars) is slightly narrower than the laser beam (points), in good agreement with the calculations of the nonorthogonal mode theory (solid line) integrating Eq. (23) over time. There are large deviations from the results of the calculations (Sec. III) of the one-mode theory and the adapted plane-wave theory (dashed and dash-dotted lines, respectively). This is expected from Sec. IV because the propagation parameter $\theta_t=2.94$ is close to π for the focused beam.

For the unfocused beam a pronounced gain narrowing of the Stokes beam is observed in Fig. 10(b). There is again good agreement of the measurements (stars) with the results of the nonorthogonal mode theory (solid line). However, the radial distribution calculated from the adapted plane-wave theory (dash-dotted line) is narrower than the measured Stokes distribution. This shows that even for the small value of $\theta_t=0.19$ of the unfocused laser beam the agreement between the measurements and the adapted plane-wave theory for the radial Stokes distribution is worse than in the case of the Stokes energy versus laser power plot in Fig. 9 (dash-dotted line for $\theta_t=0.3$). The good agreement between the measured and the calculated Stokes *energy* can be understood from the fact that the calculated [dash-dotted line in Fig. 10(b)] and the measured (stars) Stokes beam radii are substantially smaller than the laser beam radius. As a consequence, almost the complete Stokes beam is amplified in the high intensity of the center of the laser beam in both cases, leading to about the same Stokes energy.

To sum up, it has been shown in this section that the nonorthogonal mode theory is in good agreement with all experimental results for stimulated Raman scattering. The adapted plane-wave theory described correctly only the results of SRS for small propagation parameters θ_t because for the high Raman gain required for small values of θ_t the transverse variations of the Stokes beam can be neglected compared to the axial variations.

VIII. CONCLUSIONS

We investigated experimentally and theoretically Raman scattering in H_2 gas from the spontaneous to the stimulated scattering region for a Gaussian laser beam.

The results of the nonorthogonal mode theory show that the gain of the modes depends in general nonlinearly on the laser power, except for very low and very high laser power, where the usual linear power dependence of the gain is obtained. We calculated the Raman Stokes power as a function of the laser power and found that the relevant quantity is the propagation parameter θ_t, which has been introduced to account for the axial intensity distribution of the laser beam. θ_t depends on the position and length of the Raman cell and the Rayleigh range of the laser beam [Eq. (25)].

We have also addressed the question under which conditions a properly modified plane-wave theory can be used for the description of the experiments and when the more complicated nonorthogonal mode theory has to be applied. For that purpose we have compared the results of the nonorthogonal mode theory with the results of an adapted plane-wave theory and of a theory that takes into account only the lowest-order Gaussian Stokes mode (one-mode theory). For values of the propagation parameter $\theta_t \gg 1$, which can be obtained experimentally with multipass cells, there is good agreement between the nonorthogonal mode theory and the one-mode theory. In the adapted plane-wave theory the radial distribution $I_L(r)$ of the laser intensity is introduced in the exponent of the amplification term of the usual plane-wave theory. The results of this theory agree with the nonorthogonal mode theory for $\theta_t \ll 1$. Small values of θ_t can be realized experimentally in two ways. Either the cell length is short compared to the Rayleigh range or the Raman cell is located at a distance from the beam waist, which is large compared to the Rayleigh range. For intermediate values of the propagation parameter θ_t only the nonorthogonal mode theory is appropriate.

For a comparison of the calculations with the experiments, the laser beam parameters, e.g., energy, pulse duration, and beam diameter, have to be known as precisely as possible. We measured the laser beam diameter as a function of distance from the laser system and determined from these data the diameter in the beam waist and the Rayleigh range for the unfocused and the focused beam. To avoid problems with feedback by diffuse reflections, we used for SRS a H_2 cell longer than the length of the frequency-doubled Q-switched Nd:YAG laser pulse.

We measured the Raman Stokes energy of the $Q(1)$ line in H_2 gas as a function of the laser power and the radial distribution of the Stokes intensity. For the unfocused and the focused laser beam a small and a large value of the propagation parameter, respectively, were obtained. All experimental results were in good agreement with the nonorthogonal mode theory in the stimulated scattering region. The experimental results for the unfocused laser beam (small value of θ_t) agreed also with the adapted plane-wave theory. In the spontaneous Raman scattering region the nonorthogonal mode theory did not describe correctly the dependence on cell length, solid angle, and focusing conditions, but the experimental results were in agreement with the standard theory of spontaneous Raman scattering.

[1] W. Kaiser and M. Maier, in *Laser Handbook,* edited by F. T. Arecchi and E. O. Schulz-Dubois (North-Holland, Amsterdam, 1972), Vol. 2, p. 1077.

[2] A. Z. Grasyuk and I. G. Zubarev, Appl. Phys. **17**, 211 (1978).

[3] A. Penzkofer, A. Laubereau, and W. Kaiser, Prog. Quantum Electron. **6**, 55 (1979).

[4] Y. R. Shen, *The Principles of Nonlinear Optics* (Wiley-Interscience, New York, 1984), Chap. 10.

[5] M. G. Raymer and I. A. Walmsley, in *Progress in Optics,* edited by E. Wolf (North-Holland, Amsterdam, 1990), Vol. 28, p. 188.

[6] Y. R. Shen, *The Principles of Nonlinear Optics* (Ref. [4]), Chap. 17.

[7] Y. R. Shen, *The Principles of Nonlinear Optics* (Ref. [4]), Chap. 11.

[8] E. E. Hagenlocker, R. W. Minck, and W. G. Rado, Phys. Rev. **154**, 226 (1967).

[9] G. Bret and M. Denariez, Phys. Lett. **22**, 58 (1966).

[10] J. B. Grun, A. K. McQuillan, and B. P. Stoicheff, Phys. Rev. **180**, 61 (1969).

[11] A. K. McQuillan, W. R. L. Clements, and B. P. Stoicheff, Phys. Rev. A **1**, 628 (1970).

[12] P. V. Avizonis, K. C. Jungling, A. H. Guenther, and R. M. Heimlich, J. Appl. Phys. **39**, 1752 (1968).

[13] G. Haidacher and M. Maier, Proceedings of the Eighth International Quantum Electronics Conference, San Francisco, 1974 [IEEE J. Quantum Electron. **10**, 786 (1974)].

[14] S. Lögl and M. Maier, Opt. Commun. **110**, 167 (1994).

[15] B. N. Perry, P. Rabinowitz, and M. Newstein, Phys. Rev. A **27**, 1989 (1983).

[16] D. A. Cardimona, P. R. Peterson, and A. Cavrielides, Phys. Rev. A **38**, 2871 (1988).

[17] M. C. Ibison and D. C. Hanna, Appl. Phys. B **45**, 37 (1988).

[18] M. Scalora and J. W. Haus, J. Opt. Soc. Am. B **8**, 1003 (1991).

[19] S. J. Kuo, D. T. Smithey, and M. G. Raymer, Phys. Rev. Lett. **66**, 2605 (1991).

[20] P. R. Battle, J. G. Wessel, and J. L. Carlsten, Phys. Rev. A **48**, 707 (1993); Phys. Rev. Lett. **70**, 1607 (1993); J. G. Wessel, P. R. Battle, and J. L Carlsten, Phys. Rev. A **50**, 2587 (1994).

[21] D. A. Long, *Raman Spectroscopy* (McGraw-Hill, New York, 1977).

[22] H. A. Haus and S. Kawakami, IEEE J. Quantum Electron. **21**, 63 (1985).

[23] K. Petermann, IEEE J. Quantum Electron. **15**, 566 (1979).

[24] W. R. Trutna and R. L. Byer, Appl. Opt. **19**, 301 (1980), Appendix A.

[25] M. D. Duncan, R. Mahon, L. L. Tankersley, and J. Reintjes, J. Opt. Soc. Am. B **5**, 37 (1988); D. von der Linde, M. Maier, and W. Kaiser, Phys. Rev. **178**, 11 (1969).

[26] M. Maier, W. Kaiser, and J. A. Giordmaine, Phys. Rev. **177**, 580 (1969), Appendix B.

[27] W. K. Bischel and M. J. Dyer, Phys. Rev. A **33**, 3113 (1986).

[28] L. A. Rahn, R. L. Farrow, and G. J. Rosasco, Phys. Rev. A **43**, 6075 (1991).

[29] A. E. Siegman, *Lasers* (University Science Books, Mill Valley, CA, 1986), p. 276.

[30] W. K. Bischel and G. Black, in *Excimer Lasers—1983,* edited by C. K. Rhodes, H. Egger, and H. Pummer (American Institute of Physics, New York, 1983), p. 181.

[31] D. C. Hanna, D. J. Pointer, and D. J. Pratt, IEEE J. Quantum Electron. **22**, 332 (1986); H. W. Schrötter and H. W. Klöckner, in *Raman Spectroscopy of Gases and Liquids,* edited by A. Weber, Topics in Current Physics Vol. II (Springer, Berlin, 1979), p. 123.

[32] W. K. Bischel and M. J. Dyer, J. Opt. Soc. Am. B **3**, 677 (1986); J. J. Ottusch and D. A. Rockwell, IEEE J. Quantum Electron. **24**, 2076 (1988).